IEEE Access
Multidisciplinary | Rapid Review | Open Access Journal

Received April 5, 2019, accepted April 23, 2019, date of publication May 1, 2019, date of current version July 30, 2019.

Digital Object Identifier 10.1109/ACCESS.2019.2913466

Wideband MIMO Antenna Systems Based on Coupled-Loop Antenna for 5G N77/N78/N79 Applications in Mobile Terminals

ANPING ZHAO, (Senior Member, IEEE), AND ZHOUYOU REN, (Member, IEEE)
Shenzhen Sunway Communication Co., Ltd., Shenzhen 518057, China

Corresponding author: Anping Zhao (anping.zhao@sz-sunway.com)

This work was supported by the Shenzhen Science and Technology Innovation Committee under Project 20170237 and Project 20180156.

ABSTRACT A wideband 8-antenna multiple-input and multiple-output (MIMO) system that can cover 3.3–5.0 GHz is proposed for the 5G new radio N77/N78/N79 application in mobile phones. The wide bandwidth of the MIMO antenna system is obtained by the proposed coupled-loop antenna, which has three coupling sections located separately at its top central and two sides. Due to this special arrangement, the coupled-loop antenna can support three resonance modes of loop antenna: 0.5λ, 0.75λ, and 1.0λ modes. The distinctive feature of the proposed coupled-loop antenna design is that it can excite the 0.75λ modes, which has not been reported before. The wide bandwidth is obtained by the combination of the three resonance modes. To evaluate the performance of the proposed 8 × 8 MIMO antenna system, the antenna isolation, envelope correlation coefficient (ECC), and channel capacity (CC) are all investigated. Antenna prototypes for an 8-antenna MIMO system located along the edge of mobile phones are fabricated and measured, and; quite good agreements between simulation and measurement are obtained.

INDEX TERMS 5G communication, coupled-loop antenna, mobile terminal, wideband MIMO antenna system.

I. INTRODUCTION

The fifth-generation (5G) communication technology can provide many advantages such as higher transmission rate and shorter latency over the current 4G system [1], [2]. And, it has been demonstrated that to achieve high transmission rate for the 5G operations below 6GHz, the multiple-input and multiple-output (MIMO) antenna system containing a relatively large number of antennas (e.g., 8-antenna) should be adopted. Recently, many 5G MIMO antenna systems have been proposed [3]–[21]. However, these designs work only for narrow (either the single band [3]–[17] or the dual-band [18]–[21]) band operations. Very recently, 3GPP has announced [22] that the 5G New Radio (NR) will contain three working bands for the sub-6GHz application: N77 (3.3-4.2GHz), N78 (3.3-3.8 GHz), and N79 (4.4-5.0GHz). Different countries can select their own 5G bands from the above three bands. For example, China has officially announced to use the 3.3-3.6GHz and 4.8-5.0GHz bands for the 5G application [23], while the European Union (EU) has decided to adopt the 3.4-3.8GHz band [24]. Therefore, to cover all the above 5G bands for roaming purpose, it is time to develop MIMO antenna systems that can cover the entire 5G N77/N78/N79 bands (3.3-5.0GHz), as it has not been addressed by the designs proposed in [3]–[21].

Designing wideband antennas is often a challenging task, especially for mobile phones. In the past, the multi-band loop antennas that can support the low band: GSM (824-960MHz); and the high band: DCS/PCS/UMTS (1710-2170MHz), were applied successfully to mobile terminals [25]–[30]. In particular, the loop antenna supporting the low band (698-960MHz) was also proposed [30]. Among these designs, the folded loop antennas were commonly used since the size of the antennas can be significantly reduced [26]–[30]. Usually, the first three resonance modes of loop antennas are the 0.5λ, 1.0λ and 1.5λ modes. Thus, wideband cannot normally be achieved as these three resonance modes are quite far way from each other. In order to have a wideband covering the high band, tuning stub at the center of the folded loop antenna was adopted [27], [28]. In this case, the third mode (1.5λ mode)

The associate editor coordinating the review of this manuscript and approving it for publication was Zhen Gao.

is shifted toward the second mode (1.0λ mode), and thus the wideband can be achieved. To further enhance the bandwidth for both the low and high bands, the folded loop antenna that has two extra tuning sections at the left and right sides, in addition to the central tuning section, of the loop antenna was proposed [29]. In addition, the possibility in further widening the bandwidth of the high band was implicitly addressed (see Fig. 3(a) of [29]) by having three resonance modes in the high band when the three tuning sections were adopted simultaneously. Although the appearance of the three resonance modes in the high band was not clearly pointed out or discussed in [29], it was explicitly addressed in [30]. In particular, it was claimed in [30] that the 2.0λ mode of the folded loop antenna, whose resonance frequency is shifted close to that of the 1.5λ mode, can be achieved by adding one tuning section at the central and two additional tuning sections at the feeding branch of the folded loop antenna. Consequently, a wider bandwidth covering the high band (1710-2170MHz) can be obtained [30] as in this case the loop antenna supports three resonance modes: the 1.0λ, 1.5λ and 2.0λ modes; whereas the low band was covered by using a matching network.

In this paper, a novel variation of the traditional loop antenna is proposed for the application of 5G MIMO antenna system in mobile terminals. In particular, instead of adding tuning stubs at different locations of the folded loop antennas [27]–[30], a coupled-loop antenna element is established by dividing the traditional loop antenna, at its top central and two sides, into three coupling sections. With such an arrangement, the first (0.5λ) and second (1.0λ) resonance modes of the loop antenna still exist, but a new resonance mode between the first and second modes can be excited. It is demonstrated that this new resonance mode can actually be seen as the 0.75λ mode of the coupled-loop antenna, which has not been reported in the literature yet. The combination of the 0.5λ, 0.75λ, and 1.0λ modes forms a very wideband operation that can cover the whole frequency range of 3.3-5.0GHz. Based on the coupled-loop antenna element, a wideband 8-antenna MIMO system is proposed for the 5G application in mobile terminals. The performance of the MIMO antenna system is confirmed by both simulation (obtained with CST [31]) and measurement.

II. WIDEBAND 8-ANTENNA MIMO SYSTEM BASED ON THE COUPLED-LOOP ANTENNA

Fig.1 shows the perspective and side views of the wideband 8-antenna MIMO system that can cover 3.3-5.0GHz for 5G applications in the mobile phone [32]. The 8-antenna MIMO system is located along the two long edges of the mobile terminal. The dimension of the system substrate is 150mm×75mm×0.8mm. Two clearance areas (75mm×8mm) that are located separately at the top and bottom of the system substrate are reserved for the 4G LTE and other antennas used in the current phones. The eight antenna units or elements that are printed on the two small substrates are placed perpendicularly to the system substrate;

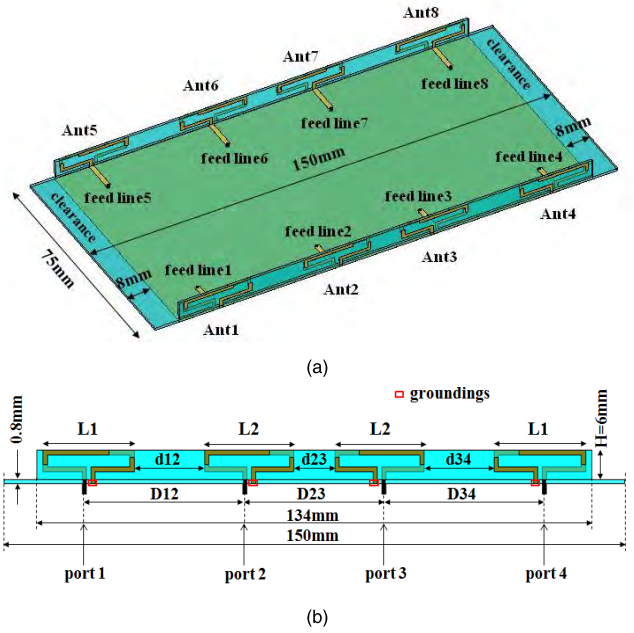

FIGURE 1. Perspective view and side view of wideband 8-antenna MIMO system. (a) Perspective view and (b) side view.

and four antenna units are placed on each side. The dimension of the small substrate is 134mm×6mm×0.8mm. The antenna height and the width of the antenna strip are fixed at 6mm and 1mm, respectively. The system substrate and the small substrate are all double-sided FR4 (with $\varepsilon_r = 4.4$ and loss tangent = 0.02). Each antenna is fed with a 50Ω microstrip line and a SMA connector through via-hole from the back side of the syste substrate. In addition, the edge-to-edge distances between Ant1 and Ant2, Ant2 and Ant3, Ant3 and Ant4 are described by d12, d23, and d34, respectively; whereas the distances between the feeds of the above antenna elements are depicted by D12, D23, and D34. Due to the symmetry, d34 = d12 and D34 = D12. And the relation between d and D are: D12 = d12 + (L1+L2)/2; and D23 = d23 + L2 + 1.0mm, L1 and L2 are the length of Ant1 (Ant4) and Ant2 (Ant3), respectively. The working principle of the proposed wideband coupled-loop MIMO antenna system will be explained by studying the single antenna element, which will be discussed next.

A. WORKING PRINCIPLE

To better understand the working principle of the proposed coupled-loop MIMO antenna system, the system consisting of only one single antenna element will be considered first. The detailed dimension and configuration of the single antenna unit or element (Ant1 is used here) is shown in Fig. 2. This antenna unit contains four radiating branches: two inner branches and two outer branches. The inner and outer branches are located on the inner and outer surfaces of the small PCB, respectively. The antenna is fed at one end of the left inner branch, and it is grounded at one end of the right outer branch. The four branches are symmetrically

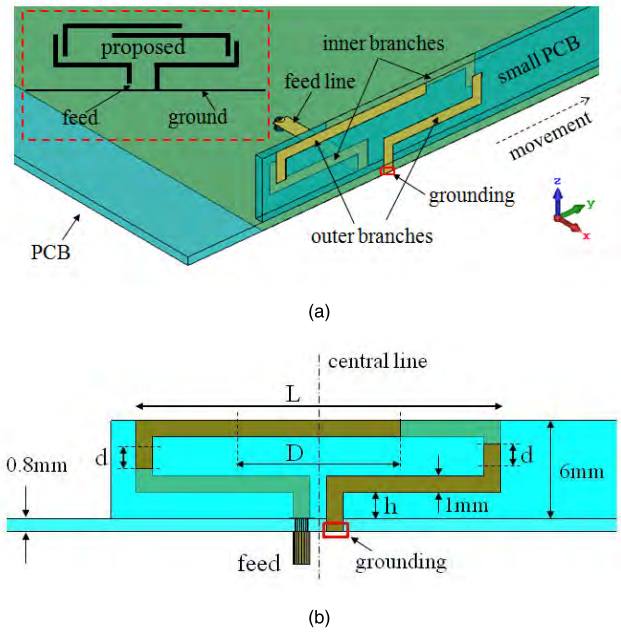

FIGURE 2. Perspective view and side view of wideband antenna system having one antenna unit only. (a) Perspective view and (b) side view.

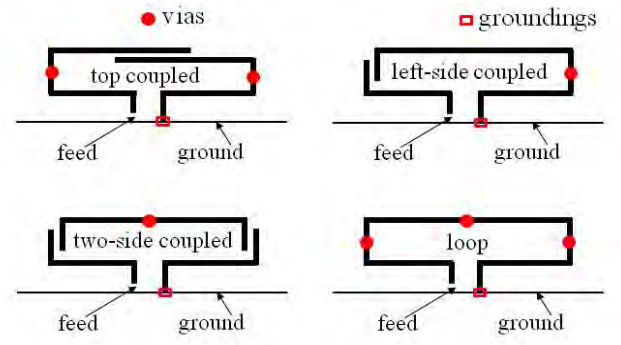

FIGURE 3. Equivalent structure of the antenna unit with different configurations.

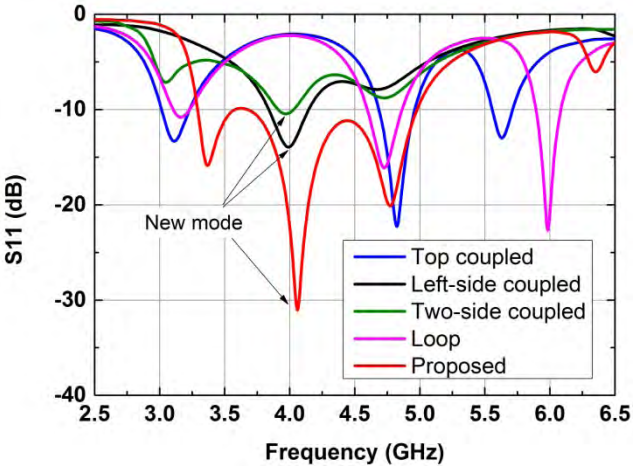

FIGURE 4. Simulated S11 of top coupled, left-side coupled, two-side coupled, loop and proposed antenna configurations.

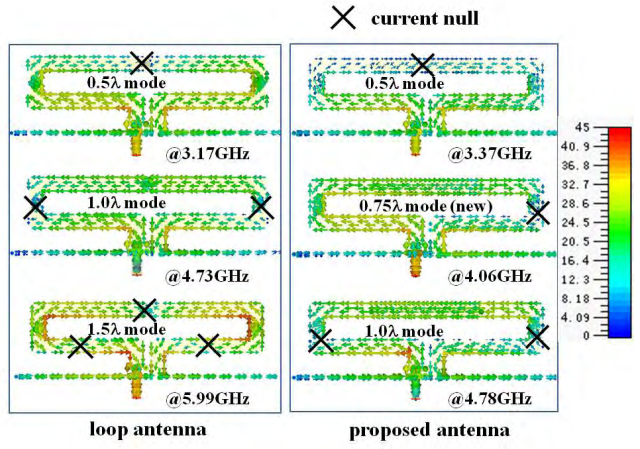

FIGURE 5. Current distributions of the first three modes of traditional loop and proposed antennas. Left: traditional loop antenna; Right: proposed antenna. All the current distributions are plotted with the same scale: 0-45dB (A/m).

located (except they are located at the two different surfaces of the small PCB) along the central line of the antenna element. There are three overlapped sections between the four branches: one of them is located at the top center of the antenna and two of them are located at the left and right sides of the antenna; and the equivalent structure of the proposed coupled-loop antenna unit is illustrated by the picture inserted inside the red-dashed frame of Fig. 2(a). The lengths of the top and side overlapped sections are described by D and d, respectively. In addition, the length of the antenna element is described by L, and the gap between the system substrate and the antenna is represented by h.

To demonstrate clearly the working principle of the proposed coupled-loop antenna, the equivalent structures of four other different antenna configurations, including the top-coupled loop, the left-side coupled loop, the two-side coupled loop and the traditional loop antennas are illustrated in Fig. 3. In order to have a fair comparison on antenna performance, all the above four antennas are varied or transformed from the proposed coupled-loop antenna. For example, the top-coupled loop antenna is obtained by setting D = 0mm and using one via (with radius R = 0.3mm, represented by the solid red dot in Fig. 3) to connect the inner and outer branches at the top center of the loop antenna; the two-side coupled loop antenna is achieved by setting d = 0mm and using one via to connect the inner and outer branches at each side of the antenna; and the left-coupled loop antenna is obtained by using one via only at the right-side of the proposed coupled-loop antenna. Finally, the loop antenna can be made with the combination of the top-coupled and two-side coupled antennas.

Fig. 4 illustrates the S_{11} of the five antennas including the proposed coupled-loop antenna and the four others shown in Fig. 3. The current distributions of the loop antenna and the proposed coupled-loop antenna are plotted in Fig. 5, in which the cross "×" represents the current null. Fig. 4 shows that

the traditional loop antenna contains three resonance modes resonating at 3.17GHz, 4.73GHz, and 5.99GHz respectively.

These three resonance modes are actually the 0.5λ, 1.0λ and 1.5λ modes of the proposed loop antenna; and the locations of the current null of these three resonance modes are shown in Fig. 5. It can also be seen from Fig. 4 that the third resonance of the loop antenna is shifted from 5.99GHz to 5.64GHz when the top-coupled antenna is used. This phenomenon is similar to the procedure used in [28] by adding a rectangular tuning patch to widen the center part of the loop antenna. Furthermore, a new mode resonating around 4.0GHz can be generated when the left-side coupled antenna is adopted. Naming this mode as the new resonance mode of the loop antenna is because it has not been reported in the literature. In addition, one can also see that the first resonance (around 3.17GHz) mode of the traditional loop antenna disappears when the left-side coupled antenna is adopted. However, this resonance mode comes back again when the two-side coupled antenna is used. Note that the impedance matching of the two-side coupled loop antenna is quite poor; yet it can be improved very significantly by the proposed coupled-loop antenna, as shown in Fig. 4.

As depicted in Fig. 4, the resonance frequencies of the first three modes of the proposed coupled-loop antenna are 3.37GHz, 4.06GHz and 4.78GHz. From the current distributions shown in Fig. 5, one can see that the first (3.37GHz) and the third (4.78GHz) resonance modes of the coupled-loop antenna are respectively equivalent to the first (3.17GHz) and the second (4.73GHz) resonance modes of the loop antenna. Therefore, the first and third resonance modes of the coupled-loop antenna work respectively as its 0.5λ and 1.0λ modes. From the results shown in Figs. 4 and 5, however, one can know that the second resonance (4.06GHz) mode of the coupled-loop antenna works as its 0.75λ mode. Although the 0.5λ and 1.0λ modes already exist in the traditional or folded loop antenna, the 0.75λ mode found in this paper does not. Hence, one can conclude that the proposed coupled-loop antenna can support its 0.5λ, 0.75λ and 1.0λ modes, whereas the other loop antennas support its 0.5λ, 1.0λ and 1.5λ modes. Most importantly, the three resonance modes, i.e., the 0.5λ, 0.75λ and 1.0λ modes, can widen the bandwidth of the coupled-loop antenna. This wider bandwidth works very well in the frequency range of 3.3-5.0GHz, which can cover all the 5G N77, N78 and N79 bands. In addition, it should be mentioned that all the above simulation results are obtained when the parameters L, D, d and h are optimized as: L = 21.5mm, D = 10mm, d = 1.5mm, and h = 1.6mm. To illustrate how the S_{11} of this antenna unit is affected by these parameters, a parameter study on S_{11} will be performed next.

B. PARAMETER STUDY

The S_{11} of the antenna unit varied as a function of D, d, h and L are plotted in Figs. 6, 7, 8 and 9, respectively. It can be seen from Fig. 6 that the value of D mainly affects the first resonance mode of the antenna unit; and the resonance frequency of this mode shifts lower when D increases. In contrast, the first and second resonance modes of the antenna unit are all affected by the value of d, as shown in Fig. 7,

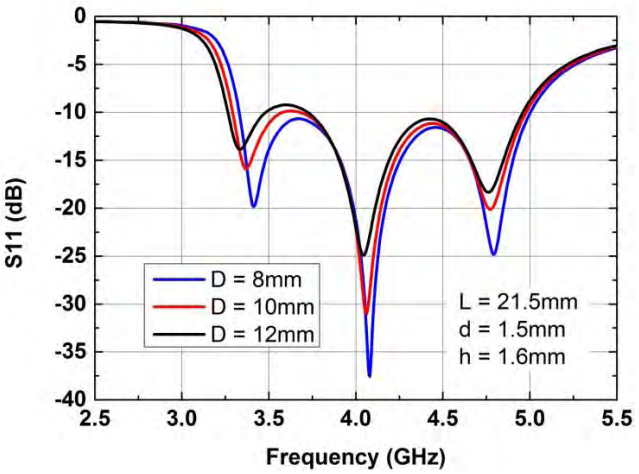

FIGURE 6. Simulated S11 of antenna unit varies as a function of D.

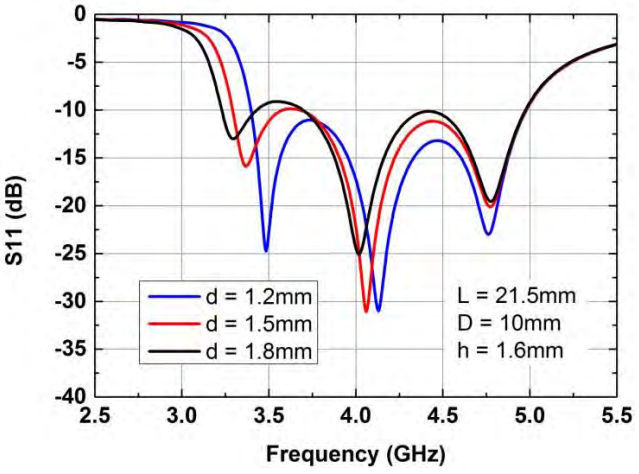

FIGURE 7. Simulated S11 of antenna unit varies as a function of d.

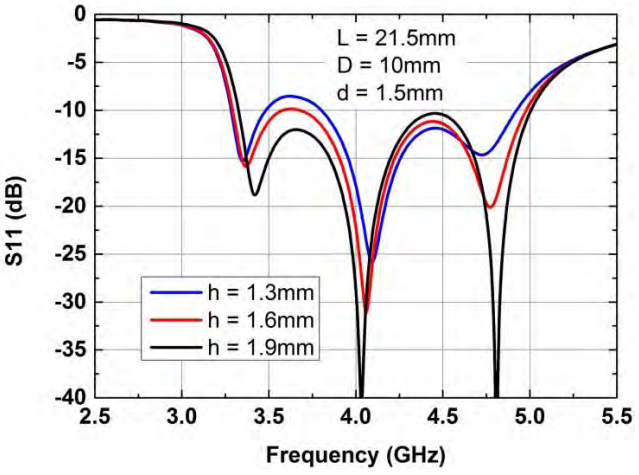

FIGURE 8. Simulated S11 of antenna unit varies as a function of h.

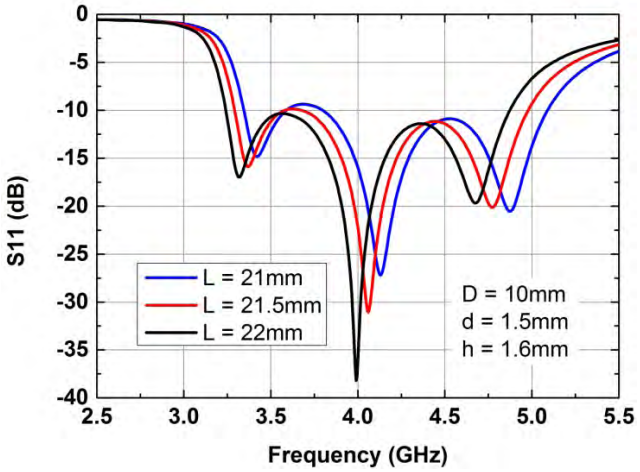

FIGURE 9. Simulated S11 of antenna unit varies as a function of L.

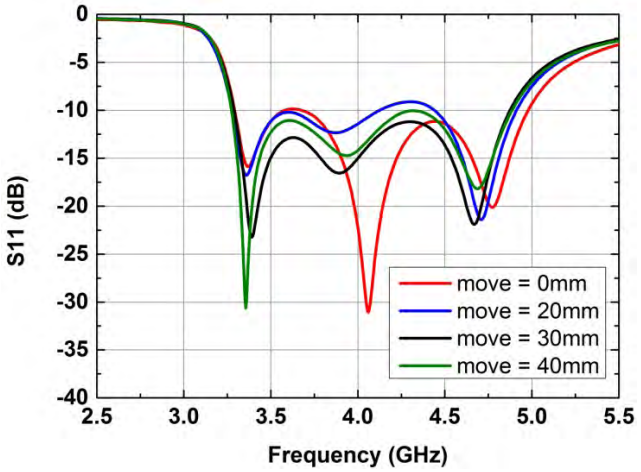

FIGURE 11. Simulated S11 of antenna unit varies as a function of location along the long edge of mobile phone.

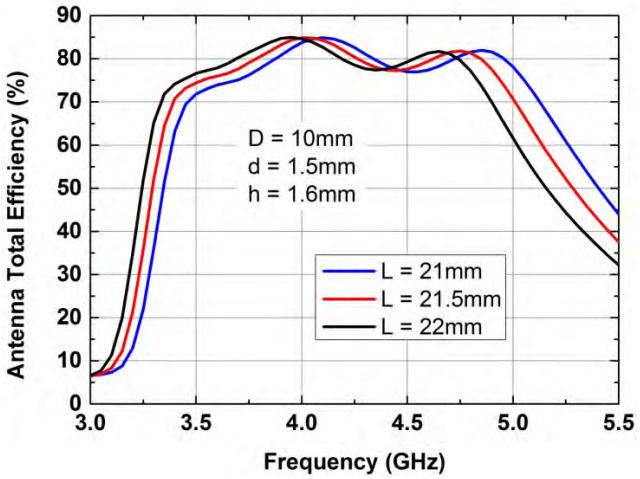

FIGURE 10. Simulated total efficiency of antenna unit varies as a function of L.

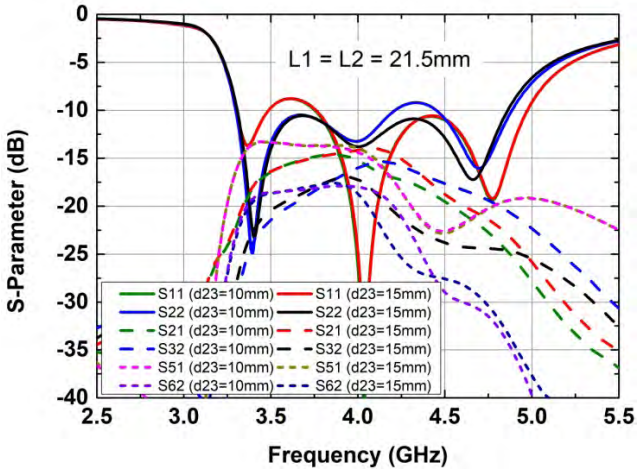

FIGURE 12. Simulated S-parameter of 8-antenna MIMO system varies as a function of d23.

which indicates that the length of the side-overlap section has quite significant impact on the antenna performance. As shown in Fig. 8, the impedance matching of the antenna unit is also strongly affected by the value of h. In addition,the results plotted in Fig. 9 demonstrate that, as expected, all the resonance frequencies of the modes decrease when the length (L) of the antenna increases. On the other hand, from the antenna S_{11} point of view, the coupled-loop antenna is optimized in 3.3-5.0GHz when L = 21.5mm.However, from the antenna efficiency point of view, good S_{11} does not always guarantee good antenna efficiency. Fig. 10 shows the antenna efficiency as a function of L. One can see from Fig. 10 that the overall antenna total efficiency in 3.3-5.0GHz is optimized while L = 22mm.Particularly, the antenna total efficiency at 3.3GHz increases from 36% to 65% when L varies from 21mm to 22mm. Such an improvement in antenna efficiency will be very useful as in general it is relatively hard to achieve good antenna efficiency for lower frequency. This will be verified again in the performance study of the proposed 8-antenna MIMO system.

In the application of the 8-antenna MIMO system in mobile terminals, it would be good if the antenna performance does not vary much when the antenna unit is moved for one position to another. This is because the possibility of adopting the same or at least very similar antenna structure at different positions can make the design procedure of MIMO antenna system easy and simple. Fig. 11 illustrates how the S_{11} of the antenna unit changes while the antenna unit is moved from its original position (i.e., move = 0mm) toward the center, along the long edge, of the mobile phone. As shown in Fig. 11, this antenna unit always works well during this shift. This can certainly be seen as one of the advantages of the proposed wideband coupled-loop antenna.

C. PEFORMANCE OF 8-ANTENNA MIMO SYSTEM

In this section, the performance of the proposed 8-antenna MIMO system shown in Fig. 1 for the 5G operation in mobile terminals will be performed and discussed. Because the MIMO antenna system has certain symmetries, only the necessary S-parameter will be presented. Also, note that the

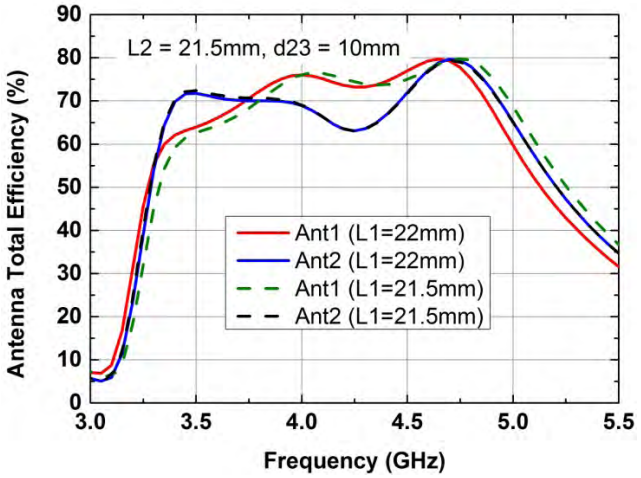

FIGURE 13. Simulated antenna total efficiency of 8-antenna MIMO system with different lengths of Ant1.

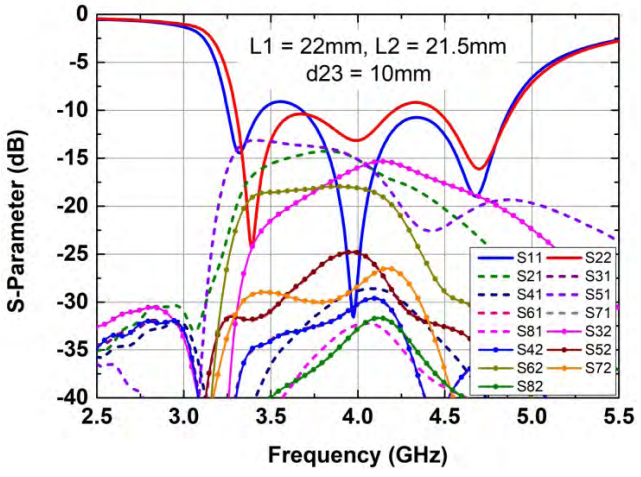

FIGURE 14. Simulated S-parameter of 8-antenna MIMO system with optimized parameters: L1 = 22mm, L2 = 21.5mm, and d23 = 10mm.

optimized parameters of D, L, d, and h used for the single antenna element will be adopted unless it is re-specified. Fig. 12 illustrates the S-parameter of the 8-anetnna MIMO system obtained with L1 = L2 = 21.5 and d23 = 10mm or 15mm. In particular, the four antennas are uniformly distributed along the long edge of the mobile phone when d23 = 15mm. Fig. 12 shows the comparison of the S-parameters between d23 = 10mm and d23 =15mm cases. Due to the symmetry, only necessary S-parameters are shown in Fig. 12. In addition, except S_{11} and S_{22}, only the isolations, S_{21}, S_{32}, S_{51} and S_{62}, that are worse than −25dB are given in Fig. 12 (see the results in Fig. 14 for reference). Among the above given isolations, the first three bad isolations are S_{51}, S_{21} and S_{32}, as can be seen from Fig. 12. The isolations between Ant1 and Ant5 (S_{51}, with a minimum value of −13.5dB at 3.4GHz) almost do not change when d23 varies from 10mm to 15mm, which is because in the above case the distance between Ant1 and Ant5 is not changed. Hence, one can only compare S_{21} and S_{32} when d23 varies. When d23 = 15mm, the minimum isolations between Ant2 and Ant1 (S_{21}) and Ant3 and Ant2 (S_{32}) are about −14dB and −17dB, respectively. This means that in this case S_{32} is 3dB better than S_{21}. We name isolation with such a difference as un-balanced isolation of the MIMO system. A balanced isolation results in good overall performance of the MIMO system. More balanced isolation can be obtained when Ant3 and Ant2 gets closer since S_{32} is better than S_{21}. As shown in Fig. 12, S_{21} = −14.7dB and S_{32} = −15.3dB while d23 = 10mm. Hence, in the rest of this work d23 = 10mm will be used as its optimal value. In addition, one can also see from Fig. 12 that, within the 3.3-5.0GHz band, the impedance matching of Ant1 at the low frequency is worse than that at the high frequency. This implies that the antenna total efficiency of Ant1 at the low frequency will not be as good as that at the high frequency, according to the conclusion drawn from the results shown in Fig. 9 and Fig. 10 for the single antenna

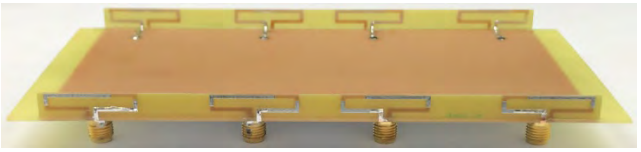

FIGURE 15. Photo of the fabricated antenna prototype of 8-antenna MIMO system with L1 = 22mm, L2 = 21.5mm, and d23 = 10mm.

unit case. Fig. 13 shows the antenna total efficiencies of Ant1 and Ant2 while the length (L1) of Ant1 (and its counterparts Ant4, Ant5 and Ant8) is with two different values. The antenna total efficiency of Ant1 at the low frequency is increased from 46% to 55% when L1 changes from 21.5mm to 22mm. Although in this case the antenna total efficiency of Ant1 at the high frequency drops from 69% to 60%, it is still good enough. The S-parameter of the 8-antenna MIMO system with its optimal parameters L1 = 22mm, L2 = 21.5mm and d23 = 10mm is plotted in Fig. 14. To give an overall view on the isolations of the 8-antenna MIMO system, all the necessary isolations are given in Fig. 14; but only S_{21}, S_{32}, S_{51} and S_{62} are worse than −25dB. It can also be seen from Fig. 14 that quite good antenna return loss and the balanced isolation (the minimum isolation values of S_{21} and S_{32} in this case are: S_{21} = −14.5dB and S_{32} = −15.2dB) within the desired working frequency band.

D. ANTENNA PROTOTYPE AND MEASUREMENT RESULTS

An antenna prototype of the proposed wideband 8-antenna MIMO system with L1 = 22mm, L2 = 21.5mm, and d23 = 10mm was fabricated and measured. The photo of the prototype is shown in Fig. 15, whereas the measured and simulated S-parameters of the antenna are plotted in Fig. 16. One can see from Fig. 16 that good agreement between the measurement and simulation is obtained. And, the measured isolation is also better than −14.5dB. The measured and simulated antenna total efficiencies and maximum antenna

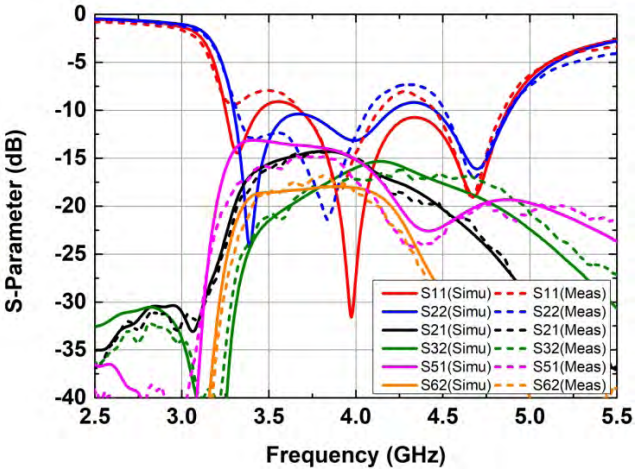

FIGURE 16. Simulated and measured S-parameter of proposed 8-antenna MIMO system.

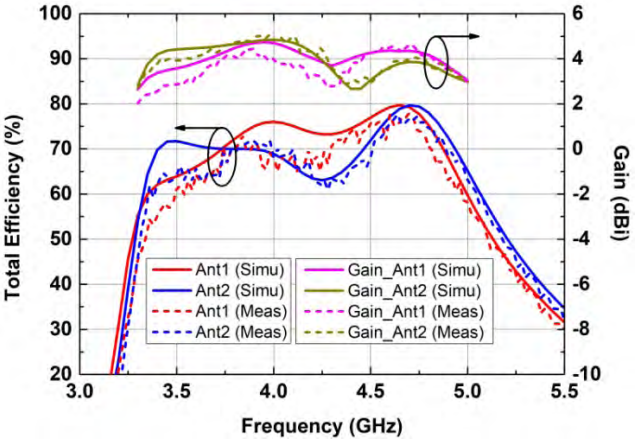

FIGURE 17. Simulated and measured antenna total efficiencies of proposed 8-antenna MIMO system.

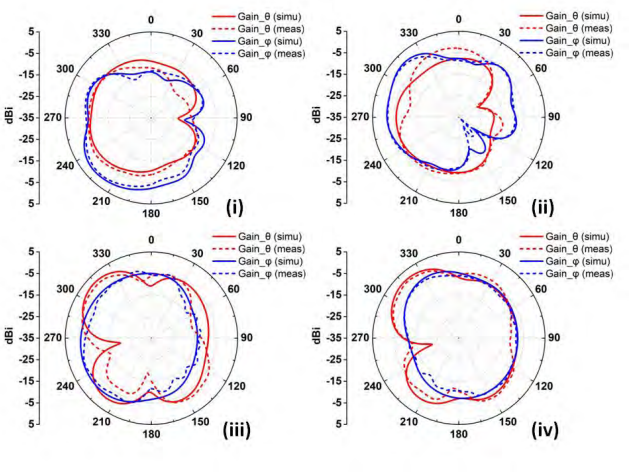

FIGURE 18. 2D antenna radiation patterns of Ant1 and Ant2 of 8-antenna MIMO system at 3.4GHz while L1 = 22mm, L2 = 21.5mm, and d23 = 10 mm. (i) Ant1 in xoy plane, (ii) Ant2 in xoy plane, (iii) Ant1 in xoz plane, and (iv) Ant2 in xoz plane.

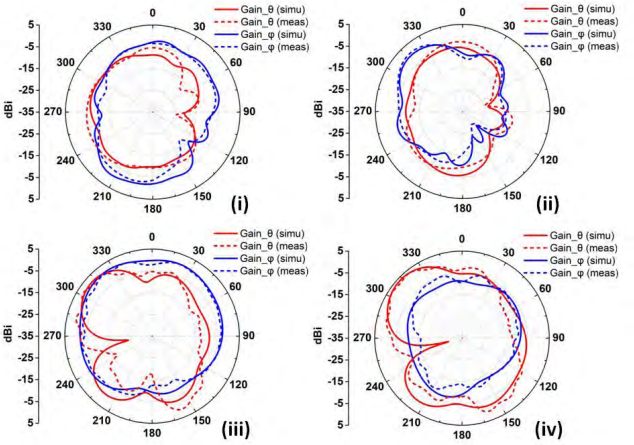

FIGURE 19. 2D antenna radiation patterns of Ant1 and Ant2 of 8-antenna MIMO system at 4.0GHz while L1 = 22mm, L2 = 21.5mm, and d23 = 10 mm. (i) Ant1 in xoy plane, (ii) Ant2 in xoy plane, (iii) Ant1 in xoz plane, and (iv) Ant2 in xoz plane.

gains are shown in Fig. 17. It can be seen from Fig. 17 that the measured antenna total efficiency and antenna gain agree well with the simulation. Within the entire 3.3-5.0GHz band, the measured antenna total efficiency is better than 46%; and the measured and simulated antenna gains are within the range of 2-5dBi. The above measured results confirm, again, that the proposed wideband 8-antenna MIMO system has not only good isolation but also good antenna total efficiency.

To further demonstrate the performance of the proposed wideband 8-antenna MIMO system, the 2D and 3D antenna radiation patterns, the envelope correlation coefficient (ECC) and the channel capacity (CC) of the MIMO system will be studied next. The simulated and measured 2D radiation patterns of Ant1 and Ant2 in the xoy and xoz planes at three different frequencies 3.4GHz, 4.0GHz and 4.8GHz are shown in Fig.18, Fig. 19 and Fig. 20, respectively; whereas the simulated 3D antenna radiation patterns of Ant1 and Ant2 are shown in Fig. 21. One can see from Figs. 18-21 that each antenna has its own unique radiation pattern; and the maximum gains of each antenna pointing to different directions at a certain frequency. Also, good agreement is obtained between simulation and measurement.

To quantitatively evaluate the performance of the proposed wideband MIMO antenna system, the envelope correlation coefficient was also analyzed. For simplification, it is assumed that multipath environment is isotropic in the sense of both power density and polarizations [33]. Therefore, the envelope correlation between antenna i and antenna j can be calculated by the complex radiation far field as follows:

$$ECC(i,j) = \frac{\left|\oint\oint A_{ij}(\theta,\varphi)\sin\theta d\theta d\varphi\right|^2}{\oint\oint A_{ii}(\theta,\varphi)\sin\theta d\theta d\varphi \cdot \oint\oint A_{jj}(\theta,\varphi)\sin\theta d\theta d\varphi} \quad (1)$$

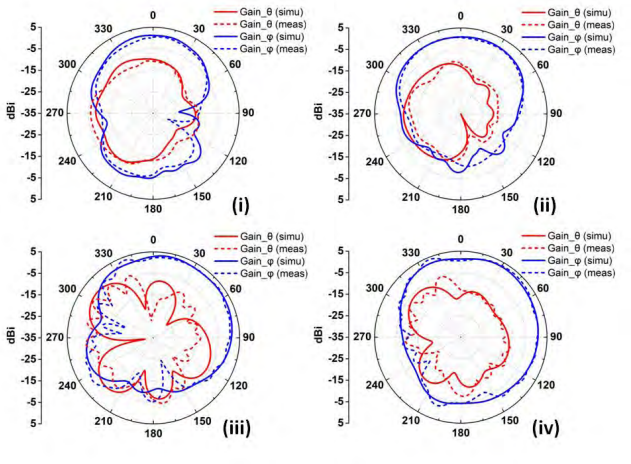

FIGURE 20. 2D antenna radiation patterns of Ant1 and Ant2 of 8-antenna MIMO system at 4.8GHz while L1 = 22mm, L2 = 21.5mm, and d23 = 10 mm. (i) Ant1 in xoy plane, (ii) Ant2 in xoy plane, (iii) Ant1 in xoz plane, and (iv) Ant2 in xoz plane.

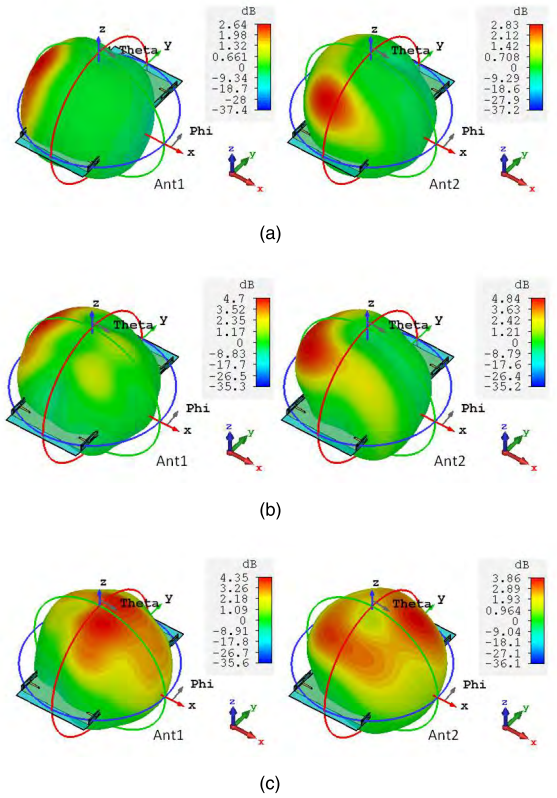

FIGURE 21. 3D antenna radiation patterns of Ant1 and Ant2 of 8-antenna MIMO system at different frequencies while L1 = 22mm,v L2 = 21.5mm, and d23 = 10mm. (a) 3.4GHz, (b) 4.0GHz, and (c) 4.8GHz.

where

$$A_{ij}(\theta,\varphi)=E_{\theta,i}(\theta,\varphi)\cdot E^{*}_{\theta,j}(\theta,\varphi)+E_{\varphi,i}(\theta,\varphi)\cdot E^{*}_{\varphi,j}(\theta,\varphi) \quad (2)$$

and the simulated and measured complex radiation far field of the antennas can be obtained from either CST or 3D measurement in an anechoic chamber.

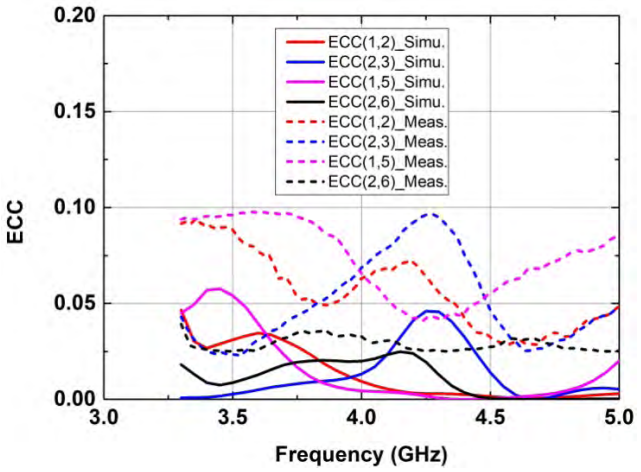

FIGURE 22. Simulated envelope correlation coefficient (ECC) of 8-antenna MIMO system with L1 = 22mm, L2 = 21.5mm, and d23 =10mm.

The simulated and measured ECC of the proposed MIMO antenna system are illustrated in Fig. 22. It should be noted here that the simulated ECC means the value of ECC is calculated from the complex radiation far field of the antennas obtained directly from CST; whereas the measured ECC means that the value of ECC is calculated from the measured complex radiation far field of the antennas. One can see that the value of the simulated ECC is smaller than 0.05 and the value of the measured ECC is smaller than 0.1 within the entire 3.3-5.0GHz band, which are all good enough for the 5G MIMO operation.

The channel capacity (CC) that is used to evaluate the performance of MIMO systems can be defined as follows:

$$CC = E\left\{log_2\left[det\left(I+\frac{SNR}{n_T}\right)H_{scale}H_{scale}T\right]\right\} \quad (3)$$

and the channel matrix H_{scale} can be calculated as follow:

$$H_{scale} = \sqrt{\rho_{scale,R\,X}}H_{i.i.d}\sqrt{\rho_{scale,TX}} \quad (4)$$

and as explained in [34], the antenna total efficiency needs to be taken into account when the channel capacity of the MIMO antenna system is calculated:

$$\rho_{scale,RX} = \sqrt{\eta_{total}}\rho_{RX}\sqrt{\eta_{total}} \quad (5)$$

The E in Eq. (3) denotes the expectation with respect to different channel realizations, I is an identity matrix, SNR is the mean signal-to-noise ratio at the receiving side, n_T is the number of transmitting antennas, and $(.)^{\mathrm{T}}$ denotes the Hermitian transpose. In this study, it is assumed that the transmitting antennas are uncorrelated (i.e., ECC = 0 at transmitting side) whereas the eight antenna elements of the proposed antenna array serve as the receiving antennas with envelope correlation coefficient ρ_{RX} (i.e., ECC) and total efficiency η_{total}. And the $H_{i.i.d}$ is an 8 × 8 matrix, in which the entries are independent identically distributed complex Gaussian variables. The simulated CC and measured CC of the 8×8 MIMO system obtained by averaging over 10,000 Rayleigh fading realizations with SNR = 20dB [3], [11], [12] are plotted

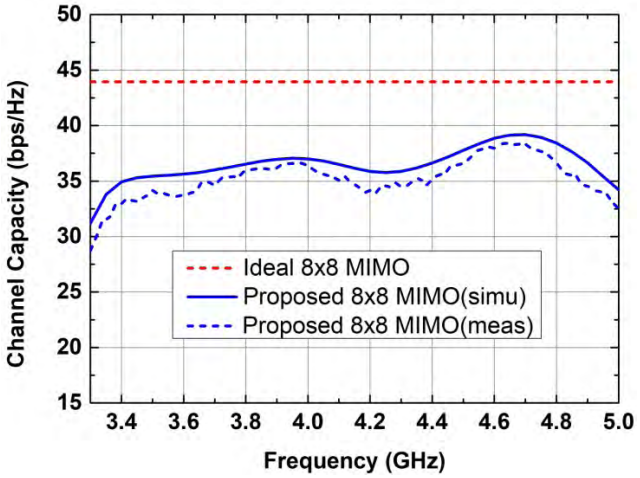

FIGURE 23. Simulated channel capacity of 8-antenna MIMO system with L1 = 22mm, L2 = 21.5mm, and d23 =10mm.

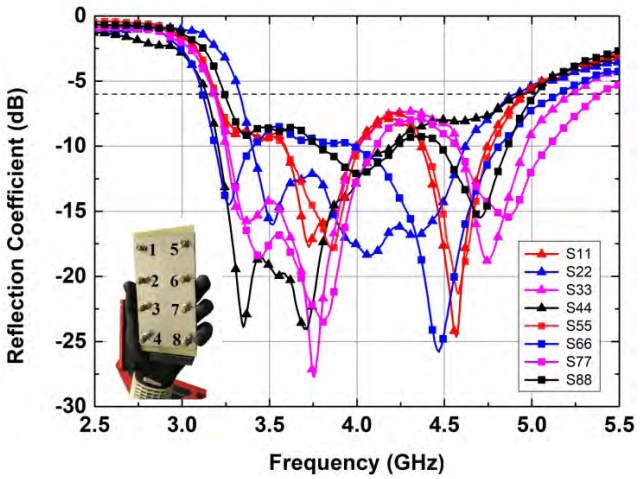

FIGURE 24. Measured antenna return loss of proposed 8-antenna MIMO system with hand.

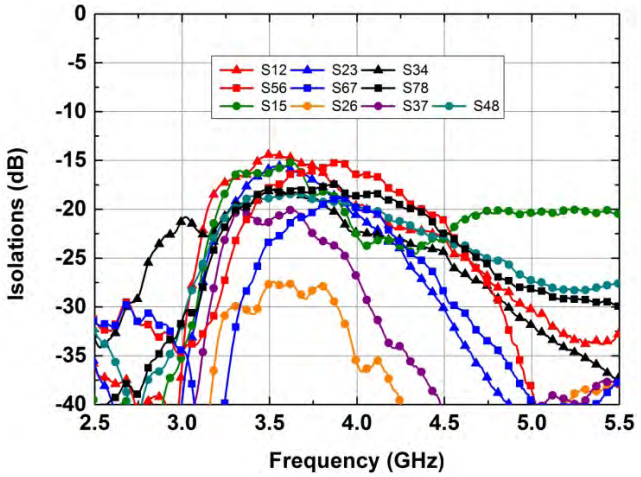

FIGURE 25. Measured antenna isolations of proposed 8-antenna MIMO system with hand.

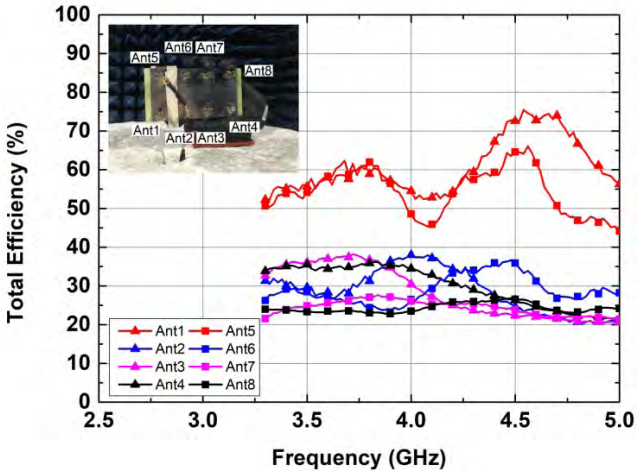

FIGURE 26. Measured antenna total efficiencies of proposed 8-antenna MIMO system with hand.

in Fig. 23. The simulated CC means that the antenna total efficiency used in Eq. (5) is obtained directly from CST. And, the measured CC means that the value of CC is calculated from the measured antenna total efficiency and the measured ECC with Eqs. (3)-(5). The value of the simulated CC in the frequency of 3.3-5.0GHz is within 31.6-39.2 bps/Hz, whereas for the ideal 8×8 MIMO antenna system it is about 44 bps/Hz. In addition, one can also see from Fig. 23 that good agreement between the simulated CC and the measured CC is achieved.

E. THE HAND EFFECT ON THE PERFORMANCE OF THE MIMO ANTENNA SYSTEM

Finally, the hand effect on the performance of the proposed 8-antenna MIMO system will be studied. The measured reflection coefficients and isolations of the proposed 8-antenna MIMO system with a phantom hand are shown in Fig. 24 and Fig. 25, respectively. And, the way of the hand to grip the antenna prototype is shown in the inserted picture of Fig. 24. In particular, Fig. 24 shows the reflection coefficients of all the eight antennas; and only the isolations between any two adjacent antennas are shown in Fig. 25. It can be seen from Fig. 24 that the measured reflection coefficients for all the other antennas are well below −6dB. And, the results in Fig. 25 show that, except for S_{12} that is very close to −15dB within a small range of frequency (around 3.5GHz), all the other isolations are better than −15dB. The above measured S-parameter results certainly indicate that the proposed 8-antenna MIMO system works fine when it is held by the phantom hand. On the other hand, how the antenna total efficiency is influenced by the phantom hand is also investigated. Fig. 26 shows the measured antenna total efficiencies of all the different antennas; and the photo of the measurement setup in a chamber is inserted in Fig. 26. Compared to the free space case, the antenna total efficiencies drop for the with hand case. In particular, the antenna with the most phantom hand coverage suffers bigger efficiency degradation,

as expected. However, one can see from the above results that when the proposed 8-antenna MIMO system is held by the phantom hand, its overall performance is still acceptable.

III. CONCLUSIONS

A wideband 8-antenna MIMO system that can cover the 3.3-5.0GHz band is proposed for the 5G application in mobile terminals. Particularly, the MIMO antenna system is based on a coupled-loop antenna element that has three coupling sections in its radiating branches: one on the top-center and two on the left- and right-side. Most importantly, due to the above special arrangement, a new resonance mode between the first resonance (0.5λ) and the second resonance (1.0λ) modes of the loop antenna is generated for the first time. As a consequence, the combination of this new mode and the first two modes of the loop antenna makes the bandwidth of the proposed coupled-loop antenna wider, which can cover all the 5G N77, N78 and N79 bands. The performance of the 8-anetnna MIMO system is confirmed by both simulation and measurement; and good MIMO antenna performance is obtained. In particular, the proposed wideband 8-antenna MIMO system shows quite high isolation, low envelope correlation coefficient, and good channel capacity, which are all good enough for practical 5G MIMO antenna application in mobile terminals. Due to the above reasons, the proposed wideband 8-antenna MIMO system could be one of the good candidates for the 5G MIMO applications in mobile phones. Consequently, the design proposed in this work not only provides good wideband 5G MIMO antenna systems for mobile applications but also rekindles the vitality of the loop antenna.

REFERENCES

[1] J. G. Andrews *et al.*, "What will 5G be?" *IEEE J. Sel. Areas Commun.*, vol. 32, no. 6, pp. 1065–1082, Jun. 2014.
[2] Y. S. Cho, J. Kim, W.-Y. Yang, and C. G. Kang, *MIMO-OFDM Wireless Communications with MATLAB*. New York, NY, USA: Wiley, 2010.
[3] A. A. Ai-Hadi, J. Ilvonen, R. Valkonen, and V. Viikari, "Eight-element antenna array for diversity and MIMO mobile terminal in LTE 3500 MHz band," *Microw. Opt. Technol. Lett.*, vol. 56, pp. 1323–1327, Jun. 2014.
[4] K. L. Wong, J. Y. Lu, L. Y. Chen, W.-Y. Li, and Y. L. Ban, "8-antenna and 16-antenna arrays using the quad-antenna linear array as a building block for the 3.5-GHz LTE MIMO operation in the smartphone," *Microw. Opt. Technol. Lett.*, vol. 58, pp. 174–181, Jan. 2016.
[5] Y.-L. Ban, C. Li, C.-Y.-D. Sim, G. Wu, and K.-L. Wong, "4G/5G multiple antennas for future multi-mode smartphone applications," *IEEE Access*, vol. 4, pp. 2981–2988, 2016.
[6] M.-Y. Li *et al.*, "Eight-port orthogonally dual-polarized antenna array for 5G smartphone applications," *IEEE Trans. Antennas Propag.*, vol. 64, no. 9, pp. 3820–3830, Sep. 2016.
[7] K.-L. Wong, C.-Y. Tsai, and J.-Y. Lu, "Two asymmetrically mirrored gap-coupled loop antennas as a compact building block for eight-antenna MIMO array in the future smartphone," *IEEE Trans. Antennas Propag.*, vol. 65, no. 4, pp. 1765–1778, Apr. 2017.
[8] H. Xu, H. Zhou, S. Gao, H. Wang, and Y. Cheng, "Multimode decoupling technique with independent tuning characteristic for mobile terminals," *IEEE Trans. Antennas Propag.*, vol. 65, no. 12, pp. 6739–6751, Dec. 2017.
[9] Z. Ren, S. Wu, and A. Zhao, "Coexist design of sub-6 GHz and millimeter-wave antennas for 5G mobile terminals," in *Proc. Int. Symp. Antennas Propag. (ISAP)*, Busan, South Korea, Oct. 2018, pp. 805–806.
[10] L. B. Sun, H. Feng, Y. Li, and Z. Zhang, "Compact 5G MIMO mobile phone antennas with tightly arranged orthogonal-mode pairs," *IEEE Trans. Antennas Propag.*, vol. 66, no. 11, pp. 6364–6369, Nov. 2018.
[11] A. Zhao and Z. Ren, "Multiple-input and multiple-output antenna system with self-isolated antenna element for fifth-generation mobile terminals," *Microw. Opt. Technol. Lett.*, vol. 61, pp. 20–27, Jan. 2019.
[12] A. Zhao and Z. Ren, "Size reduction of self-isolated MIMO antenna system for 5G mobile phone applications," *IEEE Antennas Wireless Propag. Lett.*, vol. 18, no. 1, pp. 152–156, Jan. 2019.
[13] M. Y. Li, Z. Q. Xu, Y. L. Ban, C. Y. D. Sim, and Z. F. Yu, "Eight-port orthogonally dual-polarised MIMO antennas using loop structures for 5G smartphone," *IET Microw., Antennas Propag.*, vol. 11, pp. 1810–1816, Dec. 2017.
[14] K.-L. Wong and J. Y. Lu, "3.6-GHz 10-antenna array for MIMO operation in the smartphone," *Microw. Opt. Technol. Lett.*, vol. 57, no. 7, pp. 1699–1704, Jul. 2015.
[15] J. Y. Deng, J. Yao, D. Q. Sun, and L. X. Guo, "Ten-element MIMO antenna for 5G terminals," *Microw. Opt. Technol. Lett.*, vol. 60, pp. 3045–3049, Dec. 2018.
[16] M.-Y. Li, Y.-L. Ban, Z.-Q. Xu, J. Guo, and Z.-F. Yu, "Tri-polarized 12-antenna MIMO array for future 5G smartphone applications," *IEEE Access*, vol. 6, pp. 6160–6170, Jan. 2018.
[17] C.-Y. Tsai, K.-L. Wong, and W.-Y. Li, "Experimental results of the multi-Gbps smartphone with 20 multi-input multi-output (MIMO) antennas in the 20×12 MIMO operation," *Microw. Opt. Technol. Lett.*, vol. 60, pp. 2001–2010, Aug. 2018.
[18] K. L. Wong, B. W. Lin, and W.-Y. Li, "Dual-band dual inverted-F/loop antennas as a compact decoupled building block for forming eight 3.5/5.8-GHz MIMO antennas in the future smartphone," *Microw. Opt. Technol. Lett.*, vol. 59, pp. 2715–2721, Nov. 2017.
[19] J. Guo, L. Cui, C. Li, and B. Sun, "Side-edge frame printed eight-port dual-band antenna array for 5G smartphone applications," *IEEE Trans. Antennas Propag.*, vol. 66, pp. 7412–7417, Dec. 2018.
[20] Y. Li, C. Y. D. Sim, Y. Luo, and G. Yang, "12-port 5G massive MIMO antenna array in sub-6GHz mobile handset for LTE bands 42/43/46 applications," *IEEE Access*, vol. 6, pp. 344–354, Feb. 2018.
[21] Y. Li, C.-Y.-D. Sim, Y. Luo, and G. Yang, "Multiband 10-antenna array for sub-6 GHz MIMO applications in 5-G smartphones," *IEEE Access*, vol. 6, pp. 28041–28053, Jun. 2018.
[22] *5G NR (New Radio)*. Accessed: Dec. 12, 2018. [Online]. Available: http://3gpp.org/
[23] Asia Times. (Nov. 16, 2017). *China Reserves Spectrum for 5G Services*. [Online]. Available: http://www.atimes.com/article/china-reserves-spectrum-5g-services/
[24] *Making the Best Use of Licensed and Unlicensed Spectrum*. Accessed: Dec. 10, 2018. [Online]. Available: https://www.qualcomm.com/
[25] Y. W. Chi and K. L. Wong, "Internal compact dual-band printed loop antenna for mobile phone application," *IEEE Trans. Antennas Propag.*, vol. 55, no. 5, pp. 1457–1462, May 2007.
[26] C. I. Lin and K. L. Wong, "Internal meandered loop antenna for GSM/DCS/PCS multiband operation in a mobile phone with the user's hand," *Microw. Opt. Technol. Lett.*, vol. 49, pp. 759–766, Apr. 2007.
[27] B.-K. Yu, B. Jung, H.-J. Lee, F. J. Harackiewwicz, and B. Lee, "A folded and bent internal loop antenna for GSM/DCS/PCS operation of mobile handset applications," *Microw. Opt. Technol. Lett.*, vol. 48, pp. 463–467, Mar. 2006.
[28] Y.-W. Chi and K.-L. Wong, "Compact multiband folded loop chip antenna for small-size mobile phone," *IEEE Trans. Antennas Propag.*, vol. 56, no. 12, pp. 3797–3803, Dec. 2008.
[29] K. L. Wong and C. H. Huang, "Printed loop antenna with a perpendicular feed for penta-band mobile phone application," *IEEE Trans. Antennas Propag.*, vol. 56, no. 7, pp. 2138–2141, Jul. 2008.
[30] M. Zheng, H. Y. Wang, and Y. Hao, "Internal hexa-band folded monopole/dipole/loop antenna with four resonances for mobile device," *IEEE Trans. Antennas Propag.*, vol. 60, no. 6, pp. 2880–2885, Jun. 2012.
[31] *CST Version 2018*. Accessed: Nov. 15, 2018. [Online]. Available: https://www.cst.com/
[32] A. Zhao and Z. Ren, "Wideband 5G MIMO antenna systems and mobile terminals based on coupled-loop antenna," China Patent CN 109 509 965 565 A, Mar. 22, 2019.
[33] Z. Zhang, *Antenna Design for Mobile Devices*, 2nd ed. Hoboken, NJ, USA: Wiley, 2017.
[34] J. X. Yun and R. G. Vaughan, "Multiple element antenna efficiency and its impact on diversity and capacity," *IEEE Trans. Antennas Propag.*, vol. 60, no. 2, pp. 529–539, Feb. 2012.

ANPING ZHAO (M'90–SM'98) received the B.Sc. degree in optical physics from the Changchun University of Science and Technology, China, in 1984, the M.Sc. degree in optics from the Changchun Institute of Physics, Chinese Academy of Sciences, China, in 1987, and the Ph.D. degree in electronic and electrical engineering from Brunel University, London, U.K., in 1994.

From 1987 to 1989, he was a Researcher with the Changchun Institute of Physics. In 1990, he joined the Department of Electronic and Electrical Engineering, University of Surrey, Surrey, U.K., as a Visiting Research Fellow, where he was involved in the computer verification of optical waveguide characteristics based on multiple-quantum-well (MWQ) structures in III–V semiconductor materials. In 1994, he joined the Radio Laboratory, Department of Electrical and Communications Engineering, Helsinki University of Technology, Helsinki, Finland, where he was involved in the computer-aided-design of microwave and millimeter-wave circuits with the FDTD method. He joined the Nokia Research Center, in 1997. From 1997 to 2007, he was a Senior Research Engineer/Principle Researcher with the Nokia Research Centre, Helsinki. From 2007 to 2012, he was a Principle Scientist with the Nokia Research Center, Beijing, China. In 2012, he joined Shenzhen Sunway Communication Co., Ltd., where he is the Chief Technical Expert and the Director of the Advanced Antenna Technology Department, Sunway Central Research Institute. His current research interests include antenna designs for 4G LTE, MIMO antenna systems and millimeter-wave antenna designs for 5G applications, and other antennas used in portable devices. He has authored over 120 refereed papers. He holds about 30 granted invention patents. He was listed in Marquis Who's Who in the World and Who's Who in Sciences and Engineering.

ZHOUYOU REN (M'19) received the B.Sc. degree in communication engineering from Beijing Jiaotong University, Beijing, China, in 2014, and the M.Sc. degree in data communication from The University of Sheffield, U.K., in 2016.

In 2017, he joined Shenzhen Sunway Communication Co., Ltd., as an RF Engineer. His current research interests include antenna decoupling techniques and millimeter-wave antennas, and MIMO antenna systems for 5G applications.